Investigation of the $D^0 \to K^0_S\pi^0\eta, K^0_S\pi^0\pi^0$ decays

Wei Liang,[1,*] Chu-Wen Xiao,[2,3,1,†] Guo-Mei Gan,[4] and Shi-Qi Zhou[1]

[1]*School of Physics, Hunan Key Laboratory of Nanophotonics and Devices, Central South University, Changsha 410083, China*

[2]*Department of Physics, Guangxi Normal University, Guilin 541004, China*

[3]*Guangxi Key Laboratory of Nuclear Physics and Technology, Guangxi Normal University, Guilin 541004, China*

[4]*School of Physics and Telecommunication Engineering, Yulin Normal University, Yulin 537000, China*

(Received 22 March 2026; accepted 6 August 2026; published 8 September 2026)

Inspired by the invariant mass distributions for the decays $D^0 \to K^0_S\pi^0\eta$ and $D^0 \to K^0_S\pi^0\pi^0$ reported by the BESIII Collaboration, we investigate these processes with an unified final state interaction formalism by incorporating both the S-wave pseudoscalar meson-pseudoscalar meson interactions within a chiral unitary approach and the P-wave contributions from the intermediate resonance $\bar{K}^*(892)$ and some higher states. By performing a combined fit to the invariant mass spectra and taking into account the coherence between the S and P waves, our results are in agreement with the experimental data. For the decay $D^0 \to K^0_S\pi^0\eta$, the structure near 1.0 GeV in the $\pi^0\eta$ invariant mass distribution corresponds to the signal of the $a_0(980)$, which is dynamically generated from the S-wave interactions. In the case of $D^0 \to K^0_S\pi^0\pi^0$, the near-threshold enhancement in the $\pi^0\pi^0$ mass distribution arises from the combined contributions of the $f_0(500)$ and the intermediate $\bar{K}^*(892)$, while the cusplike structure around $1\mathrm{GeV}^2$ is associated with the $f_0(980)$.

DOI: 10.1103/2slf-x5kp

I. INTRODUCTION

The study of strong-interaction dynamics in the low-energy region of particle physics remains a core challenge in understanding the nonperturbative nature of quantum chromodynamics (QCD) [1–6]. In this regime, the QCD coupling constant becomes large, rendering perturbative methods unreliable. To reveal the nonperturbative QCD behavior, the hadronic decays of charm mesons provide a valuable opportunity to investigate the interplay between the short-distance weak interactions and the long-distance strong dynamics [7–12]. In particular, the final state interaction among two of the outgoing pseudoscalar mesons for three-body charm meson decays can generate abundant resonance structures in the invariant mass spectra, which not only provide insights into the weak decay mechanisms of charm quarks but also serve as sensitive probes of the complex dynamics underlying final state strong interactions.

Among the long-standing open issues in light-hadron spectroscopy, the nature of the scalar states $f_0(500)$, $f_0(980)$, and $a_0(980)$ remains one of the most intriguing and enduring puzzles; see more discussions in the review of the meson resonances below 1 GeV from the Particle Data Group (PDG) [3] and the discussions in Refs. [13–18]. Given their unusual properties, especially the proximity of the states $f_0(980)$ and $a_0(980)$ to the $K\bar{K}$ threshold, these states have been interpreted within various theoretical frameworks, including conventional $q\bar{q}$ mesons, compact tetraquarks, hadronic molecules, and hybrids involving multiple components [19–29]. Against this backdrop, the chiral unitary approach offers a natural and successful theoretical framework, where the low-lying scalar resonances emerge dynamically from the unitarized S-wave interactions of coupled pseudoscalar meson channels, rather than being introduced *ad hoc* as elementary Breit-Wigner resonances [26,30–33].

Experimentally, the BESIII, *BABAR*, Belle, and CLEO Collaborations reported many experimental measurements about three-body decays of the charm hadrons, such as in the Refs. [34–40], which provide a good opportunity to investigate these light scalar mesons [41–47] with their results on the two-body spectra of the final states $\pi\pi$, $\pi\eta$, and/or $K\bar{K}$. Recently, the BESIII Collaboration reported their precise measurements of the decays $D^0 \to K^0_S\pi^0\eta$ [48] and $D^0 \to K^0_S\pi^0\pi^0$ [49]. In Ref. [48], they performed an amplitude analysis of the decay $D^0 \to K^0_S\pi^0\eta$ and obtained the branching fraction $\mathcal{B}(D^0 \to K^0_S\pi^0\eta) = (1.016 \pm 0.013_{\mathrm{stat}} \pm 0.014_{\mathrm{syst}})\%$,

*Contact author: 212201014@csu.edu.cn
†Contact author: xiaochw@gxnu.edu.cn

together with $\mathcal{B}(D^0 \to K_S^0 a_0(980)^0, a_0(980)^0 \to \pi^0\eta) = (9.88 \pm 0.37_{\rm stat} \pm 0.42_{\rm syst}) \times 10^{-3}$, showing that the contribution from the resonances $a_0(980)^0$ and $\bar{K}^*(892)$ plays a dominant role in the decay procedure. This decay channel was first observed by the CLEO Collaboration [50], where the results with a Dalitz-plot analysis indicated the dominant contributions from the subdecays $K_S^0 a_0(980)$ and $K^*(892)\eta$. In Ref. [49], the BESIII Collaboration reported the measurement results of the decay $D^0 \to K_S^0\pi^0\pi^0$ with an amplitude analysis using 20.3fb^{-1} of e^+e^- data collected at $\sqrt{s} = 3.773$GeV, where they measured the branching ratio as $\mathcal{B}(D^0 \to K_S^0\pi^0\pi^0) = (1.026 \pm 0.008_{\rm stat} \pm 0.009_{\rm syst})\%$ and found that the dominant intermediate process was $D^0 \to \bar{K}^*(892)^0\pi^0$ with significant contribution from the S-wave component. For this decay channel, the CLEO Collaboration had also performed a Dalitz analysis and found that the data required contributions associated with the resonances $K^*(892)$, $f_0(980)$ and the broad one $\sigma/f_0(500)$ [51].

On the theoretical side, the decays $D^0 \to K_S^0\pi^0\eta$ and $D^0 \to K_S^0\pi^0\pi^0$ are particularly attractive to investigate the resonance properties of these scalar states $f_0(500)$, $f_0(980)$, and $a_0(980)$, since the $\pi^0\eta$ system is an ideal channel to observe the isovector state $a_0(980)$, while the $\pi^0\pi^0$ system filters isoscalar configurations and is sensitive to $f_0(500)$ and $f_0(980)$. Indeed, using a final state interaction framework based on the chiral unitary approach, the decays $D^0 \to K_S^0 f_0(500)$, $D^0 \to K_S^0 f_0(980)$, and $D^0 \to K_S^0 a_0(980)$ were studied in Ref. [52] with a weak-interaction diagram of dominant W-internal emission, where they predicted that the signals of these scalar resonances could be found in the spectra of the $\pi^+\pi^-$ and $\pi^0\eta$ in the final states $\bar{K}^0\pi^+\pi^-$ and $\bar{K}^0\pi^0\eta$, respectively. With an analogous formalism, the decay $D^0 \to \bar{K}^0\pi^0\pi^0$ was investigated in Ref. [53] with the contributions from the S-wave resonance $f_0(500)$ and $f_0(980)$ of the final state interaction and the intermediate P-wave state $\bar{K}^*(892)$. In their analyzed results to the data of the CLEO Collaboration [51], the near-threshold enhancement in the $\pi^0\pi^0$ spectrum was attributed mainly by $f_0(500)$ and $K^*(892)$, while the cusplike structure around 1 GeV was associated with the $f_0(980)$ signal. Furthermore, as discussed in Ref. [54], even though the decay processes are similar, the $a_0(980)$ signal in the $\pi\eta$ spectra is different. Indeed, in Ref. [54], they found the clean signal of $a_0(980)$ in the final state interaction of the decay $D^+ \to \bar{K}^0\pi^+\eta$ as observed in the BESIII Collaboration's measurements [35,55], due to no contribution from the low-lying $\bar{K}^*$ resonance. This is different from the similar decay process $D^0 \to K^-\pi^+\eta$ as investigated in the previous work [31], where they found that the line shape of the $a_0(980)$ signal was substantially distorted by the interference effect of the low-lying $\bar{K}^*$ resonances as observed in the Belle experiment [56].

With the recent measurements of the BESIII Collaboration [48,49], we investigate the decays $D^0 \to K_S^0\pi^0\eta$ and $D^0 \to K_S^0\pi^0\pi^0$ within a unified dynamical framework of the weak interaction, where the final state interaction is treated in the coupled channel approach, which dynamically generates the scalar resonances as meson-meson molecular states. In this way, the $\pi^0\pi^0$ and $\pi^0\eta$ invariant mass distributions can be analyzed with the same formalism, allowing us to clarify the respective roles of the resonances $f_0(500)$, $f_0(980)$, and $a_0(980)$. Our manuscript is organized as following. In Sec. II, we introduce the final state interaction formalism for the decays $D^0 \to K_S^0\pi^0\eta$ and $D^0 \to K_S^0\pi^0\pi^0$. The results of combined fit for corresponding invariant mass distributions are presented in Sec. III. Finally, a short summary is shown in Sec. IV.

II. FORMALISM

We investigate the $D^0 \to K_S^0\pi^0\eta$ and $D^0 \to K_S^0\pi^0\pi^0$ reactions through the internal-W emission diagram, which is shown in Fig. 1. The quark c of the initial state D^0 can decay into the s quark by emitting W^+ boson, while the quark $\bar{u}$ acts as a spectator and remains unchanged. There are two ways of hadronization. One way is that the $s\bar{d}$ quarks form the final state $\bar{K}^0$ directly, and the quark pair $u\bar{u}$ hadronizes within the pair $(u\bar{u} + d\bar{d} + s\bar{s})$ created from the vacuum. The other one is that the $u\bar{u}$ become the π^0/η, and the $s\bar{d}$ undergo the hadronization. Note that, in our cases, there is no contribution from the external-W emission diagram, since the π^0/η cannot be created in this diagram, which is different from the cases of similar decays $D^+ \to \bar{K}^0\pi^+\eta$ and $D^0 \to K^-\pi^+\eta$ [31,54].

As done in Ref. [57], the hadronization can start from the matrix M with elements $q\bar{q}$,

$$M = \begin{pmatrix} u\bar{u} & u\bar{d} & u\bar{s} \\ d\bar{u} & d\bar{d} & d\bar{s} \\ s\bar{u} & s\bar{d} & s\bar{s} \end{pmatrix}. \tag{1}$$

Hence, the hadronization of the components $u\bar{u}$ and $s\bar{d}$ can be written as

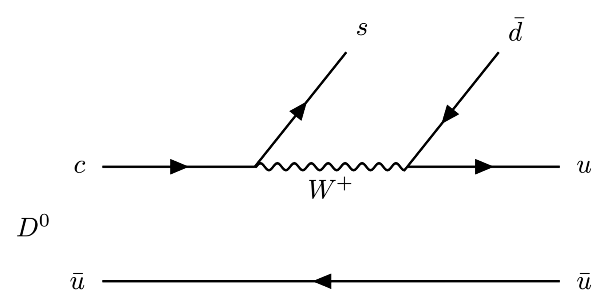

FIG. 1. The internal-W emission mechanism for the decays $D^0 \to K_S^0\pi^0\eta$ and $D^0 \to K_S^0\pi^0\pi^0$.

$$u(\bar{u}u + \bar{d}d + \bar{s}s)\bar{u} = (M \cdot M)_{11}, \qquad s(\bar{u}u + \bar{d}d + \bar{s}s)\bar{d} = (M \cdot M)_{32}. \tag{2}$$

Then, the elements of matrix M can be rewritten in terms of the pseudoscalar meson fields ϕ [31,58–61],

$$\phi = \begin{pmatrix} \frac{1}{\sqrt{2}}\pi^0 + \frac{1}{\sqrt{3}}\eta + \frac{1}{\sqrt{6}}\eta' & \pi^+ & K^+ \\ \pi^- & -\frac{1}{\sqrt{2}}\pi^0 + \frac{1}{\sqrt{3}}\eta + \frac{1}{\sqrt{6}}\eta' & K^0 \\ K^- & \bar{K}^0 & -\frac{1}{\sqrt{3}}\eta + \frac{\sqrt{2}}{\sqrt{3}}\eta' \end{pmatrix}. \tag{3}$$

In fact, the matrix M in SU(3) should be $\phi + \frac{1}{\sqrt{3}}\mathrm{diag}(\eta_1, \eta_1, \eta_1)$, where the η_1 is a singlet, taking into account the standard mixing between η and η'. The term $\frac{1}{\sqrt{3}}\mathrm{diag}(\eta_1, \eta_1, \eta_1)$ is omitted because the structure $[\phi, \partial_\mu\phi]$ in the chiral Lagrangians render this term inoperative. In Refs. [52,62], this ordinary matrix ϕ of the chiral perturbation theory is also used. Then, all the possible meson-meson components in Eq. (2) are given by

$$(M \cdot M)_{11} = \frac{1}{2}\pi^0\pi^0 + \frac{1}{3}\eta\eta + \frac{2}{\sqrt{6}}\pi^0\eta + \pi^+\pi^- + K^+K^-, \qquad (M \cdot M)_{32} = K^-\pi^+ - \frac{1}{\sqrt{2}}\bar{K}^0\pi^0, \tag{4}$$

where we ignore the contributions of η' in our calculation as done in Ref. [31] because it has a large mass and does not play a role in the generation of $f_0(980)/a_0(980)$.

Therefore, the hadronization processes for the decays $D^0 \to K_S^0\pi^0\eta$ and $D^0 \to K_S^0\pi^0\pi^0$ as shown in Fig. 1 can be expressed as

$$\begin{aligned} H &= V_p V_{cs} V_{ud}\left[(s\bar{d} \to \bar{K}^0)[M_{11} \to (M \cdot M)_{11}] + \left(u\bar{u} \to \frac{1}{\sqrt{2}}\pi^0\right)[M_{32} \to (M \cdot M)_{32}] \right. \\ &\quad \left. + \left(u\bar{u} \to \frac{1}{\sqrt{3}}\eta\right)[M_{32} \to (M \cdot M)_{32}]\right] \\ &= V_p V_{cs} V_{ud}\left[\frac{1}{3}\bar{K}^0\eta\eta + \frac{1}{\sqrt{6}}\bar{K}^0\pi^0\eta + \pi^+\pi^-\bar{K}^0 + K^+K^-\bar{K}^0 + \frac{1}{\sqrt{2}}\pi^0K^-\pi^+ + \frac{1}{\sqrt{3}}\eta K^-\pi^+\right] \\ &= C_1\left[\frac{1}{3}\bar{K}^0\eta\eta + \frac{1}{\sqrt{6}}\bar{K}^0\pi^0\eta + \pi^+\pi^-\bar{K}^0 + K^+K^-\bar{K}^0 + \frac{1}{\sqrt{2}}\pi^0K^-\pi^+ + \frac{1}{\sqrt{3}}\eta K^-\pi^+\right], \end{aligned} \tag{5}$$

where the factor $C_1 = V_p V_{cs} V_{ud}$ is a global parameter, which absorbs the production vertex V_p and the elements of the Cabibbo-Kobayashi-Maskawa matrix $V_{cs}V_{ud}$ and can be obtained by fitting experimental data as done in our former works [18,63–65]. Note that C_1 also absorbs the normalization factor when fitting the experimental data in events. It is obvious that the final states $\bar{K}^0\pi^0\eta$ not only can produce from hadronization processes directly, but also can generate from the rescattering procedure of the final state interactions with the other terms, while $\bar{K}^0\pi^0\pi^0$ are only obtained from rescattering effect, which is shown in Figs. 2 and 3, respectively. Therefore, considering the same W-internal emission mechanism of Fig. 1, the amplitudes of the $D^0 \to K_S^0\pi^0\eta$ and $D^0 \to K_S^0\pi^0\pi^0$ decay processes in the S wave can be written as

$$\begin{aligned} t(s_{12}, s_{23})_{D^0 \to \bar{K}^0\pi^0\eta} &= \frac{1}{\sqrt{6}}C_1 + \frac{1}{\sqrt{6}}C_1 G_{\pi^0\eta}(s_{23}) T_{\pi^0\eta \to \pi^0\eta}(s_{23}) + C_1 G_{K^+K^-}(s_{23}) T_{K^+K^- \to \pi^0\eta}(s_{23}) \\ &\quad + \frac{1}{\sqrt{6}}C_1 G_{\bar{K}^0\eta}(s_{23}) T_{\bar{K}^0\eta \to \bar{K}^0\eta}(s_{13}) + \frac{1}{\sqrt{2}}C_1 G_{K^-\pi^+}(s_{13}) T_{K^-\pi^+ \to \bar{K}^0\eta}(s_{13}) \\ &\quad + \frac{1}{3}C_1 G_{\bar{K}^0\eta}(s_{12}) T_{\bar{K}^0\eta \to \bar{K}^0\pi^0}(s_{12}) + \frac{1}{\sqrt{6}}C_1 G_{\bar{K}^0\pi^0}(s_{12}) T_{\bar{K}^0\pi^0 \to \bar{K}^0\pi^0}(s_{12}) \\ &\quad + \frac{1}{\sqrt{3}}C_1 G_{K^-\pi^+}(s_{12}) T_{K^-\pi^+ \to \bar{K}^0\pi^0}(s_{12}), \end{aligned} \tag{6}$$

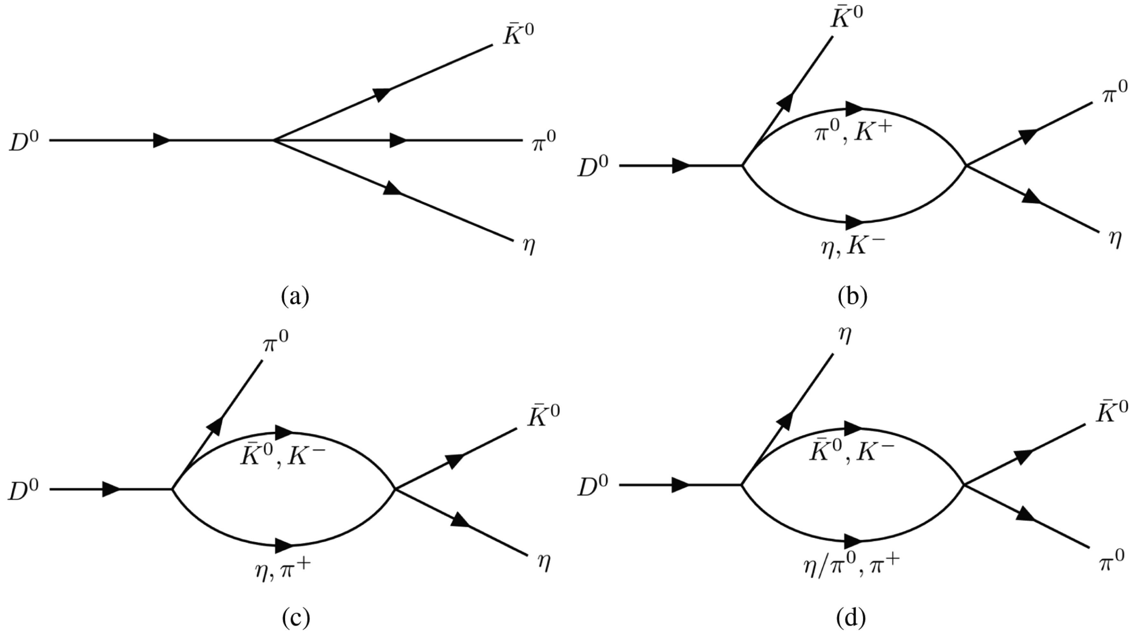

FIG. 2. Diagrammatic representations of rescattering for the decay $D^0 \to K_S^0\pi^0\eta$. (a) Tree-level production. (b) Rescattering of $\pi^0\eta$ *and* K^+K^-. (c) Rescattering of $\bar{K}^0\eta$ and $K^-\pi^+$. (d) Rescattering of $\bar{K}^0\eta, \bar{K}^0\pi^0,$ *and* $K^-\pi^+$.

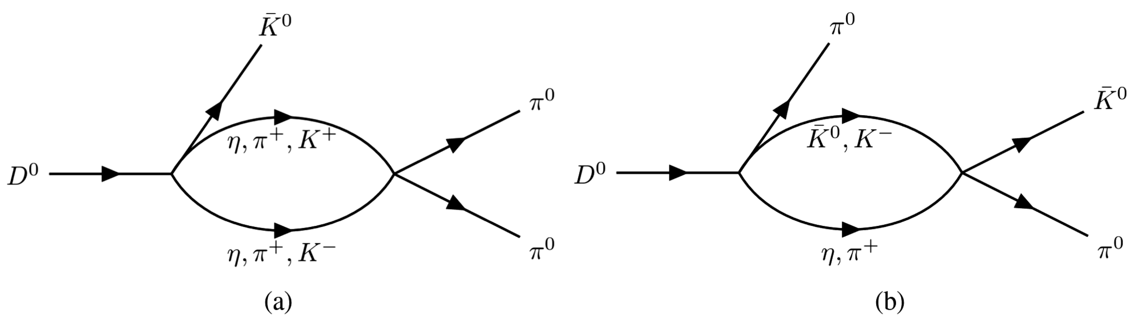

FIG. 3. Diagrammatic representations of rescattering for the decay $D^0 \to K_S^0\pi^0\pi^0$. (a) Rescattering of $\eta\eta$, $\pi^+\pi^-\eta,$ *and* K^+K^-. (b) Rescattering of $\bar{K}^0\eta$ and $K^-\pi^+$.

$$\begin{aligned} t(s_{12}, s_{23})_{D^0\to\bar{K}^0\pi^0\pi^0} = {}& \frac{1}{3}\times 8C_1 G_{\eta\eta}(s_{23})T_{\eta\eta\to\pi^0\pi^0}(s_{23}) + 2C_1 G_{\pi^+\pi^-}(s_{23})T_{\pi^+\pi^-\to\pi^0\pi^0}(s_{23}) \\ & + 2C_1 G_{K^+K^-}(s_{23})T_{K^+K^-\to\pi^0\pi^0}(s_{23}) + \frac{1}{\sqrt{6}}C_1 G_{\bar{K}^0\eta}(s_{12})T_{\bar{K}^0\eta\to\bar{K}^0\pi^0}(s_{12}) \\ & + \frac{1}{\sqrt{2}}C_1 G_{K^-\pi^+}(s_{12})T_{K^-\pi^+\to\bar{K}^0\pi^0}(s_{12}). \end{aligned} \tag{7}$$

The s_{ij} is the energy of two-body system, which is defined as $s_{ij} = (p_i + p_j)^2$, with p_i and p_j as the four-momenta of these two particles. The indices $i, j = 1, 2, 3$ represent three final states of K_S^0, π^0, and η/π^0, respectively. Note that it should be an extra factor $1/2$ for the loop function of the system $\eta\eta$ with identical particles [66] in Eq. (7), as commented in Refs. [52,53], which has been canceled with a factor of 2 for generating two identical particles [63,64,67]. However, with the unitary normalization, there is a factor $1/4$ containing the amplitude $T_{\eta\eta\to\pi^0\pi^0}$ compared to the physical one, due to two pairs of identical particles in the initial and final states. Thus, in view of these reasons, we take a factor 8 for the term of $G_{\eta\eta}T_{\eta\eta\to\pi^0\pi^0}$ to recover the physical amplitude. Analogously, a factor 2 is multiplied to the terms of $T_{\pi^+\pi^-\to\pi^0\pi^0}$ and $T_{K^+K^-\to\pi^0\pi^0}$, see Eq. (7). Additionally, we take $|K_S^0\rangle = \frac{1}{\sqrt{2}}(|K^0\rangle - |\bar{K}^0\rangle)$ into account as done in Ref. [68] and change the final state from $\bar{K}^0$ to K_S^0; the S-wave amplitude in Eqs. (6) and (7) can be revised as

$$
\begin{aligned}
t(s_{12},s_{23})_{D^0\to K_S^0\pi^0\eta} = {} & \frac{-1}{2\sqrt{3}}C_1 - \frac{1}{2\sqrt{3}}C_1 G_{\pi^0\eta}(s_{23})T_{\pi^0\eta\to\pi^0\eta}(s_{23}) - \frac{1}{\sqrt{2}}C_1 G_{K^+K^-}(s_{23})T_{K^+K^-\to\pi^0\eta}(s_{23}) \\
& + \frac{1}{2\sqrt{6}}C_1 G_{\bar{K}^0\eta}(s_{23})T_{\bar{K}^0\eta\to\bar{K}^0\eta}(s_{13}) - \frac{1}{2}C_1 G_{K^-\pi^+}(s_{13})T_{K^-\pi^+\to\bar{K}^0\eta}(s_{13}) \\
& + \frac{1}{6}C_1 G_{\bar{K}^0\eta}(s_{12})T_{\bar{K}^0\eta\to\bar{K}^0\pi^0}(s_{12}) + \frac{1}{2\sqrt{6}}C_1 G_{\bar{K}^0\pi^0}(s_{12})T_{\bar{K}^0\pi^0\to\bar{K}^0\pi^0}(s_{12}) \\
& - \frac{1}{\sqrt{6}}C_1 G_{K^-\pi^+}(s_{12})T_{K^-\pi^+\to\bar{K}^0\pi^0}(s_{12}),
\end{aligned} \tag{8}
$$

$$
\begin{aligned}
t(s_{12},s_{23})_{D^0\to K_S^0\pi^0\pi^0} = {} & \frac{-1}{3\sqrt{2}}\times 8C_1 G_{\eta\eta}(s_{23})T_{\eta\eta\to\pi^0\pi^0}(s_{23}) - \frac{1}{\sqrt{2}}\times 2C_1 G_{\pi^+\pi^-}(s_{23})T_{\pi^+\pi^-\to\pi^0\pi^0}(s_{23}) \\
& - \frac{1}{\sqrt{2}}\times 2C_1 G_{K^+K^-}(s_{23})T_{K^+K^-\to\pi^0\pi^0}(s_{23}) + \frac{1}{2\sqrt{6}}C_1 G_{\bar{K}^0\eta}(s_{23})T_{\bar{K}^0\eta\to\bar{K}^0\pi^0}(s_{13}) \\
& - \frac{1}{2}C_1 G_{K^-\pi^+}(s_{13})T_{K^-\pi^+\to\bar{K}^0\pi^0}(s_{13}),
\end{aligned} \tag{9}
$$

where $G_{PP'}$ and $T_{PP'}$ are the loop functions and the two-body scattering amplitudes, respectively; see some more details below. Note that, for the decay $D^0 \to K_S^0\pi^0\eta$, the $\bar{K}^0\eta$ rescattering is disregarded as done in Ref. [54] for the process $D^+ \to \bar{K}^0\pi^+\eta$ due to its threshold far away from the energy region of the $\kappa/K_0^*(700)$.

The scattering amplitudes in Eqs. (8) and (9) can be calculated by solving the coupled channel Bethe-Salpeter equation [30,69],

$$
T = [1 - VG]^{-1}V, \tag{10}
$$

where the matrix V is composed by the scattering potentials of corresponding coupled channel. In the chiral unitary approach, the interaction potentials can be evaluated from the chiral Lagrangians. For the isospin $I = 0$ sector, V is a 5×5 matrix of the interaction kernel for five channels: $\pi^+\pi^-(1)$, $\pi^0\pi^0(2)$, $K^+K^-(3)$, $K^0\bar{K}^0(4)$, and $\eta\eta(5)$, and the explicit expressions for these elements are given by [62–64,70]

$$
\begin{aligned}
& V_{11} = -\frac{1}{2f^2}s, \qquad V_{12} = -\frac{1}{\sqrt{2}f^2}(s - m_\pi^2), \qquad V_{13} = -\frac{1}{4f^2}s, \\
& V_{14} = -\frac{1}{4f^2}s, \qquad V_{15} = -\frac{1}{3\sqrt{2}f^2}m_\pi^2, \qquad V_{22} = -\frac{1}{2f^2}m_\pi^2, \\
& V_{23} = -\frac{1}{4\sqrt{2}f^2}s, \qquad V_{24} = -\frac{1}{4\sqrt{2}f^2}s, \qquad V_{25} = -\frac{1}{6f^2}m_\pi^2, \\
& V_{33} = -\frac{1}{2f^2}s, \qquad V_{34} = -\frac{1}{4f^2}s, \\
& V_{35} = -\frac{1}{12\sqrt{2}f^2}(9s - 6m_\eta^2 - 2m_\pi^2), \qquad V_{44} = -\frac{1}{2f^2}s, \\
& V_{45} = -\frac{1}{12\sqrt{2}f^2}(9s - 6m_\eta^2 - 2m_\pi^2), \\
& V_{55} = -\frac{1}{18f^2}(16m_K^2 - 7m_\pi^2),
\end{aligned} \tag{11}
$$

where $f = 0.093\mathrm{GeV}$ is the pion decay constant [26], and m_P are the corresponding masses of pseudoscalar mesons which are taken from PDG [3]. For the $I = 1/2$ sector, three channels are coupled, $K^-\pi^+(1)$, $\bar{K}^0\pi^0(2)$, $\bar{K}^0\eta(3)$, and then the elements of the 3×3 symmetric matrix are given by [31,33,63]

$$
\begin{aligned}
V_{11} &= \frac{-1}{6f^2}\left[\frac{3}{2}s - \frac{3}{2s}(m_\pi^2 - m_K^2)^2\right],\\
V_{12} &= \frac{1}{2\sqrt{2}f^2}\left[\frac{3}{2}s - m_\pi^2 - m_K^2 - \frac{(m_\pi^2 - m_K^2)^2}{2s}\right],\\
V_{13} &= \frac{1}{2\sqrt{6}f^2}\left[\frac{3}{2}s - \frac{7}{6}m_\pi^2 - \frac{1}{2}m_\eta^2 - \frac{1}{3}m_K^2 + \frac{3}{2s}(m_\pi^2 - m_K^2)(m_\eta^2 - m_K^2)\right],\\
V_{22} &= \frac{-1}{4f^2}\left[-\frac{s}{2} + m_\pi^2 + m_K^2 - \frac{(m_\pi^2 - m_K^2)^2}{2s}\right],\\
V_{23} &= -\frac{1}{4\sqrt{3}f^2}\left[\frac{3}{2}s - \frac{7}{6}m_\pi^2 - \frac{1}{2}m_\eta^2 - \frac{1}{3}m_K^2 + \frac{3}{2s}(m_\pi^2 - m_K^2)(m_\eta^2 - m_K^2)\right],\\
V_{33} &= -\frac{1}{4f^2}\left[-\frac{3}{2}s - \frac{2}{3}m_\pi^2 + m_\eta^2 + 3m_K^2 - \frac{3}{2s}(m_\eta^2 - m_K^2)^2\right].
\end{aligned}
\tag{12}
$$

For the $I = 1$ sector, three channels are coupled, $K^+K^-(1)$, $K^0\bar{K}^0(2)$, $\pi^0\eta(3)$, and then the elements of the 3×3 symmetric matrix are given by [54,71]

$$
\begin{aligned}
V_{11} &= -\frac{1}{2f^2}s, \qquad V_{12} = -\frac{1}{4f^2}s, \qquad V_{13} = -\frac{1}{3\sqrt{6}f^2}[3s - 2m_K^2 - m_\eta^2],\\
V_{22} &= -\frac{1}{2f^2}s, \qquad V_{23} = \frac{1}{3\sqrt{6}f^2}[3s - 2m_K^2 - m_\eta^2], \qquad V_{33} = -\frac{2}{3f^2}m_\pi^2.
\end{aligned}
\tag{13}
$$

Note that the unitary normalizations $|\eta\eta\rangle \to \frac{1}{\sqrt{2}}|\eta\eta\rangle$ and $|\pi^0\pi^0\rangle \to \frac{1}{\sqrt{2}}|\pi^0\pi^0\rangle$ are accounted for the identical particles, which have been taken into account in the interaction potentials; thus, there is no extra factor for the G functions in Eq. (10) [62,66]. Generally, the loop function G is logarithmically divergent, we adopt three-momentum cutoff method to solve this problem, and the explicit form is given by [33]

$$
G(s) = \frac{1}{16\pi^2 s}\left\{\sigma\left(\arctan\frac{s+\Delta}{\sigma\lambda_1} + \arctan\frac{s-\Delta}{\sigma\lambda_2}\right) - \left[(s+\Delta)\ln\frac{(1+\lambda_1)q_{\max}}{m_1} + (s-\Delta)\ln\frac{(1+\lambda_2)q_{\max}}{m_2}\right]\right\}, \tag{14}
$$

where $\sigma = [-(s-(m_1+m_2)^2)(s-(m_1-m_2)^2)]^{1/2}$, $\Delta = m_1^2 - m_2^2$, and $\lambda_i = \sqrt{1 + m_i^2/q_{\max}^2}$ ($i = 1, 2$). $q_{\max}$ is the cutoff momentum, and we take the value as 650 MeV, which was also used in Ref. [71] for the case of considering the η-η' mixing.

Additionally, in the chiral unitary approach, the most reliable range of the S-wave pseudoscalar meson-pseudoscalar meson interactions is up to 1.1~1.2 GeV. In order to make reasonable calculations, we smoothly extrapolate $G(s)T(s)$ above the energy cut $\sqrt{s} \geq \sqrt{s_{\mathrm{cut}}} = 1.1\mathrm{GeV}$, as done in Ref. [14],

$$
G(s)T(s) = G(s_{\mathrm{cut}})T(s_{\mathrm{cut}})e^{-\alpha(\sqrt{s}-\sqrt{s_{\mathrm{cut}}})}, \qquad \sqrt{s} > \sqrt{s_{\mathrm{cut}}}, \tag{15}
$$

where G and T are the loop functions and amplitudes that are introduced in Eqs. (14) and (10), respectively. The α is the smoothing extrapolation factor, of which the value is obtained by fitting experimental data. Furthermore, one can use different parametrizations for Eq. (15) to check the smooth extrapolation. Note that, in the chiral unitary approach, the imaginary part of the loop function is equal to the phase space of the two-body system [72], which means that the imaginary part of the loop function is well defined with the s dependence. Thus, for Eq. (15) one can keep the s dependence of the imaginary part of $G(s)$ and let its real part calculate with the s_{cut}. On the other hand, we make further tests as done in Ref. [14] with fixed values of $\alpha = 3.7, 5.4, 7.7\mathrm{GeV}^{-1}$ for Eq. (15). With the tests of these two parametrizations, we find that there is no improvement to the fitted results, or even worse, and thus we keep using the one of Eq. (15).

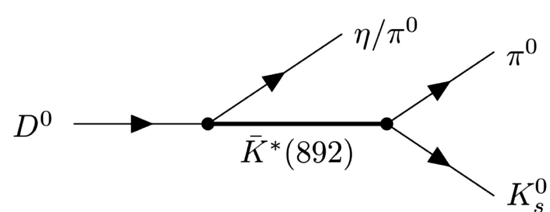

FIG. 4. Mechanism for the $D^0 \to K_S^0\pi^0\eta$ and $D^0 \to K_S^0\pi^0\pi^0$ decays via the intermediate vector meson $\bar{K}^*(892)$.

TABLE I. Values of the parameters from the combined fit for the data of the decay $D^0 \to K_S^0\pi^0\pi^0$ observed by the BESIII Collaboration [49].

Parameters	C_1	α	D	$\alpha_{\bar{K}^*(892)}$	D_1	$\alpha'_{\bar{K}^*(892)}$	$\chi^2/\mathrm{d.o.f.}$
Fit	1486.15	−2.03	−118.09	−3.91	523.46	−7.88	35.38

In addition to the contributions from the S-wave pseudoscalar meson-pseudoscalar menson interactions, we also considered the contribution from the intermediate vector meson $\bar{K}^*(892)$ for the primary hint, where the higher resonances' contributions will be discussed in the next section. The mechanism is depicted in Fig. 4, and the amplitude for the process $D^0 \to \bar{K}^*(892)\pi^0 \to \bar{K}^0\pi^0\pi^0$ can be calculated by [31,73]

$$\begin{aligned}\mathcal{M}_{\bar{K}^*(892)}(s_{12}, s_{23}) &= \frac{\mathcal{D}e^{i\alpha_{\bar{K}^*(892)}}}{s_{12} - M^2_{\bar{K}^*(892)} + iM_{\bar{K}^*(892)}\Gamma_{\bar{K}^*(892)^+}} \\ &\times \left[\frac{(m^2_{D^0} - m^2_{\eta/\pi^0})(m^2_{\bar{K}^0} - m^2_{\pi^0})}{M^2_{\bar{K}^*(892)}} - s_{13} + s_{23}\right], \end{aligned} \tag{16}$$

where D and $\alpha_{\bar{K}^*}(892)$ are the normalization factor and phase, respectively, which can be determined by fitting the experimental data. $M_{\bar{K}^*(892)}$ and $\Gamma_{\bar{K}^*(892)}$ are the mass and width of the intermediate state $\bar{K}^*(892)$, of which the values are taken from the PDG as 0.89167 and 0.0514 GeV [3]. Note that the s_{ij} are not independent and fulfill the following constraint condition:

$$s_{12} + s_{13} + s_{23} = m^2_{D^0} + m^2_{\bar{K}^0} + m^2_{\pi^0} + m^2_{\eta/\pi^0}. \tag{17}$$

Hence, there are only two s_{ij} that are independent. The total amplitudes of the $D^0 \to K_S^0\pi^0\eta$ and $D^0 \to K_S^0\pi^0\pi^0$ processes that contain the contributions from the S and P wave can be written as

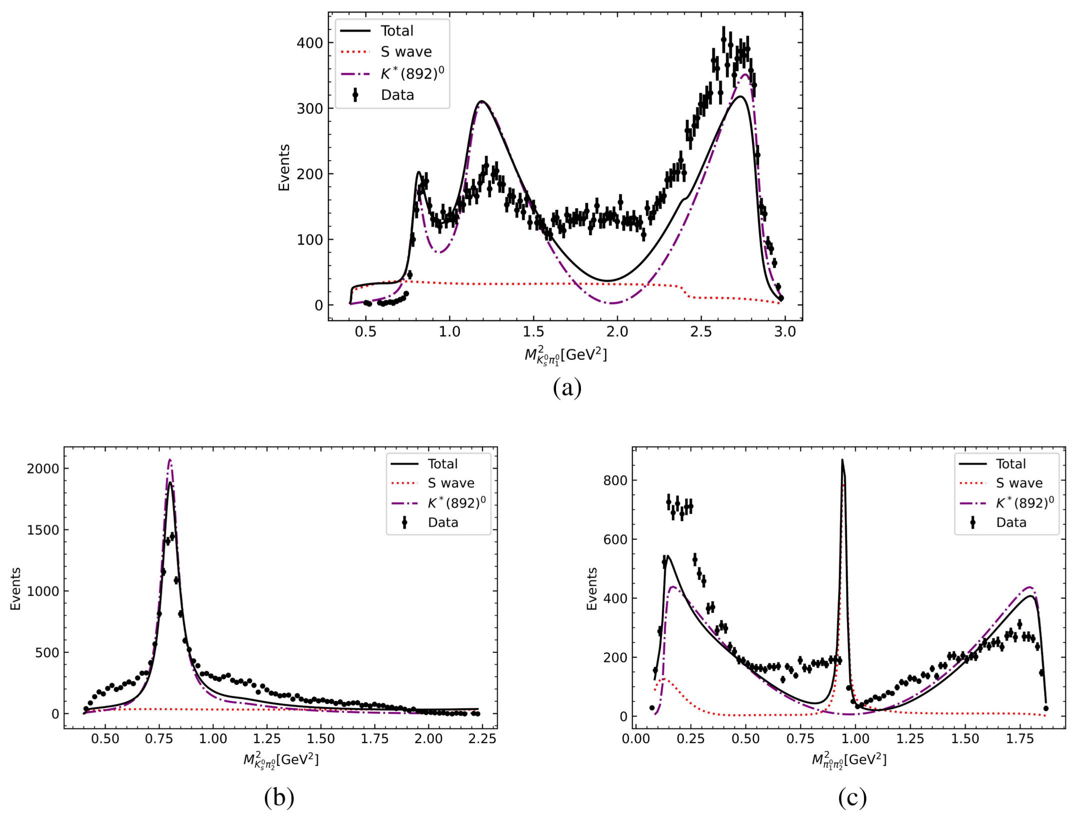

FIG. 5. Combined fit for the invariant mass distributions of the decay $D^0 \to K_S^0\pi^0\pi^0$. The solid (black) line is the total contributions of the S and P waves, the dashed (red) line represents the S-wave contributions, the dash-dotted (purple) line means the contributions of the $\bar{K}^*(892)$ in the P wave. The dotted (black) points are the experimental data measured by the BESIII Collaboration [49]. (a) Invariant mass distribution of $K_S^0\pi_1^0$. (b) Invariant mass distribution of $K_S^0\pi_2^0$. (c) Invariant mass distribution of $\pi_1^0\pi_2^0$.

TABLE II. Values of the parameters from the combined fit for the data of the decay $D^0 \to K_S^0\pi^0\pi^0$ with the energy-dependent parametrization of Eq. (22).

Parameters	C_1	α	D	D'	$\alpha_{\bar{K}^*(892)}$	D_1	D'_1	$\alpha'_{\bar{K}^*(892)}$	χ^2/d.o.f.
Fit	−831.70	12.54	1837.68	−2440.53	−1.81	−235.76	−305.45	−3.79	10.81

$$t'(s_{12}, s_{23})_{D^0\to K_S^0\pi^0\eta} = t(s_{12}, s_{23})_{D^0\to K_S^0\pi^0\eta} + \mathcal{M}_{\bar{K}^*(892)}(s_{12}, s_{23}), \tag{18}$$

$$t'(s_{12}, s_{23})_{D^0\to K_S^0\pi^0\pi^0} = t(s_{12}, s_{23})_{D^0\to K_S^0\pi^0\pi^0} + \mathcal{M}_{\bar{K}^*(892)}(s_{12}, s_{23}) + (2 \leftrightarrow 3). \tag{19}$$

Note that, when considering the identical particles in $D^0 \to K_S^0\pi^0\pi^0$ decay, the parameters in the contributions of the P wave are different: there are four parameters and, thus, two normalizations D/D_1 and two phases $\alpha_{\bar{K}^*(892)}/\alpha'_{\bar{K}^*(892)}$.

Finally, the double differential width distribution of these two three-body decays are written as

$$\frac{d^2\Gamma}{ds_{12}ds_{23}} = \frac{1}{(2\pi)^3}\frac{1}{32m_{D^0}^3}|t'(s_{12}, s_{23})_{D^0\to K_S^0\pi^0\eta}|^2, \tag{20}$$

$$\frac{d^2\Gamma}{ds_{12}ds_{23}} = \frac{1}{(2\pi)^3}\frac{1}{32m_{D^0}^3}\frac{1}{2}|t'(s_{12}, s_{23})_{D^0\to K_S^0\pi^0\pi^0}|^2, \tag{21}$$

where the factor $\frac{1}{2}$ origins from the identical particle π^0 in final states, and the $t'(s_{12}, s_{23})$ is the total amplitudes that are presented in Eqs. (18) and (19). With the constraint condition given by Eq. (17), one can calculate the invariant mass distributions $d\Gamma/ds_{12}$, $d\Gamma/ds_{23}$, and $d\Gamma/ds_{23}$ by integrating over the other variable with the limit of the Dalitz plot, where more detail can be found in PDG [3].

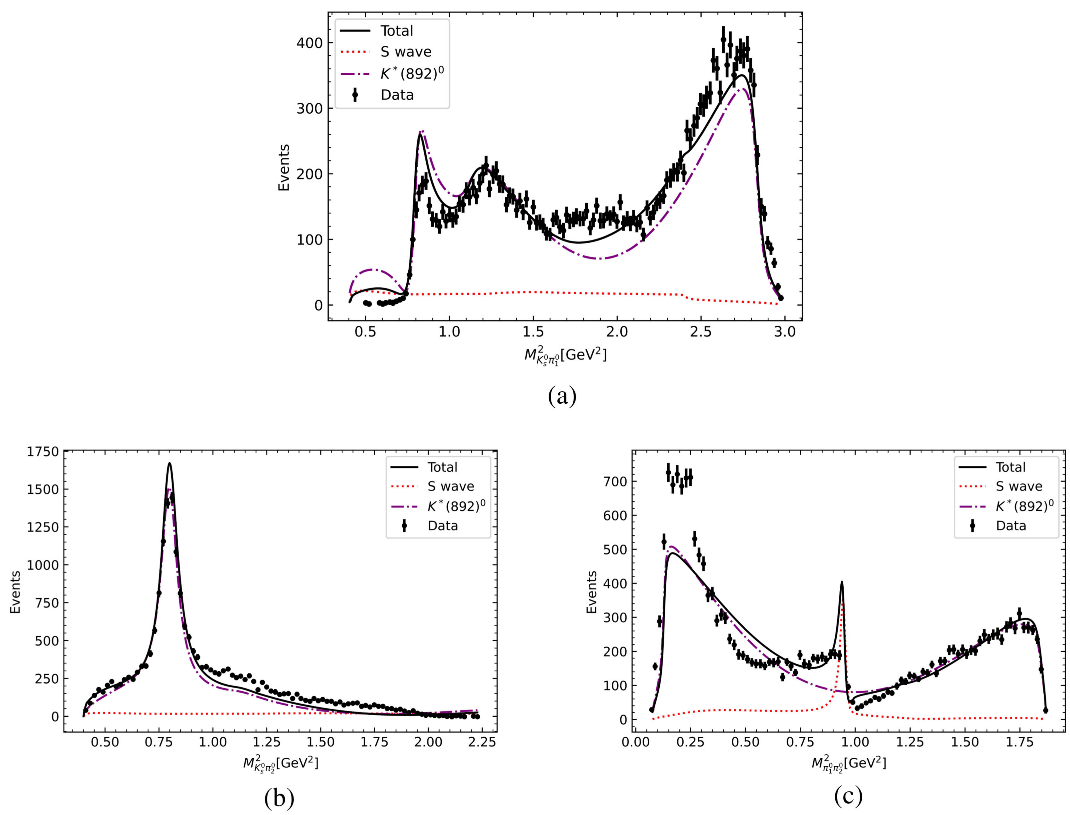

(a) (b) (c)

FIG. 6. Combined fit for the invariant mass distributions of the decay $D^0 \to K_S^0\pi^0\pi^0$ with the energy-dependent parametrization of Eq. (22). The solid (black) line is the total contributions of the S and P waves, the dashed (red) line represents the S-wave contributions, the dash-dotted (purple) line means the contributions of the $\bar{K}^*(892)$ in the P wave. The dotted (black) points are the experimental data measured by the BESIII Collaboration [49]. (a) Invariant mass distribution of $K_S^0\pi_1^0$. (b) Invariant mass distribution of $K_S^0\pi_2^0$. (c) Invariant mass distribution of $\pi_1^0\pi_2^0$.

TABLE III. Values of the parameters from the combined fit for the data of the decay $D^0 \to K^0_S\pi^0\pi^0$ with the $\bar{K}^*(1680)$ contributed.

Parameters	C_1	α	D	$\alpha_{\bar{K}^*(892)}$	D_1	$\alpha'_{\bar{K}^*(892)}$	$D_{\bar{K}^*(1680)}$	$\alpha_{\bar{K}^*(1680)}$	$D_{1,\bar{K}^*(1680)}$	$\alpha'_{\bar{K}^*(1680)}$	χ^2/d.o.f.
Fit	869.39	9.14	−139.34	−3.17	498.44	−7.00	2796.28	−3.88	2062.10	−1.92	12.99

III. RESULTS AND DISCUSSIONS

In our formalism discussed above, there are several parameters that need to be determined by fitting the experimental data. For the $D^0 \to K^0_S\pi^0\eta$ process, there are four parameters, the global parameter C_1, the extrapolation parameter α, the normalization parameters D, and phases $\alpha_{\bar{K}^*(892)}$ in the P-wave amplitude. For the $D^0 \to K^0_S\pi^0\pi^0$ decay, due to the identical particles, there are two more parameters for the P wave, D_1 and $\alpha'_{\bar{K}^*(892)}$. As shown in Eqs. (18) and (19), the coherence of the amplitudes between the S and P waves are taken into account.

For the $D^0 \to K^0_S\pi^0\pi^0$ decay, through the interference between the S and P waves, we perform a combined fit to the experimental data from three corresponding invariant mass distributions measured by the BESIII Collaboration [49]; the free parameters and mass distributions are shown in Table I and Fig. 5, respectively, where, as done in the experiments [49], the two pions are distinguished by momentum, named π^0_1 and π^0_2 for the high and low momentum pions, respectively. In Fig. 5(a), the $K^0_S\pi^1_0$ distribution is depicted, where three obvious structures mainly benefit from the vector meson $\bar{K}^*(892)$, and the contribution from the S wave is relatively small. In Fig. 5(b), our results for the $K^0_S\pi^0_2$ mass distribution is in agreement with the BESIII measurements. The narrow peak structure around 0.75GeV^2 is contributed from the vector meson $\bar{K}^*(892)$ in the P wave, while the contribution from the S-wave pseudoscalar meson-pseudoscalar interactions is just shown as a smooth background in this distribution. For the $\pi^0_1\pi^0_2$ invariant mass distribution as presented in Fig. 5(c), the structure around 0.25GeV^2 is the contribution of the scalar meson $f_0(500)$ in the S wave and the reflection of the vector

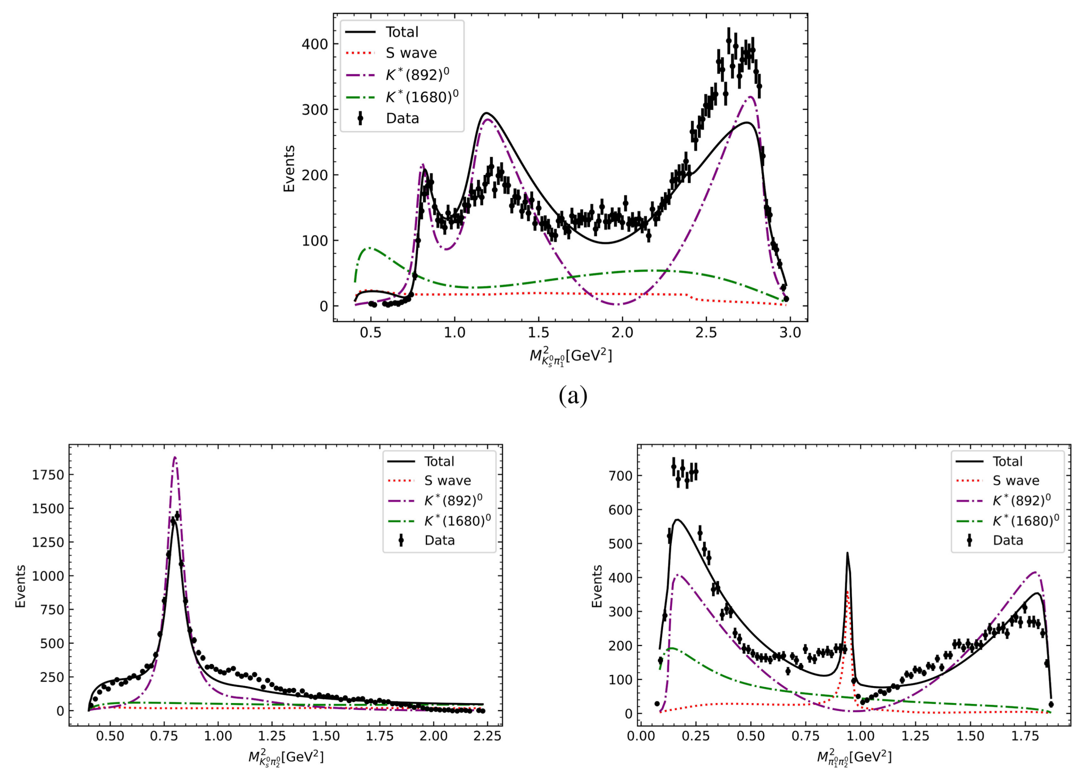

FIG. 7. Combined fit for the invariant mass distributions of the decay $D^0 \to K^0_S\pi^0\pi^0$ with the $\bar{K}^*(1680)$ contributed. The solid (black) line is the total contributions of the S and P waves, the dashed (red) line represents the S-wave contributions, the dash-dotted (purple) line means the contributions of the $\bar{K}^*(892)$ in the P wave. The dotted (black) points are the experimental data measured by the BESIII Collaboration [49]. (a) Invariant mass distribution of $K^0_S\pi^0_2$. (b) Invariant mass distribution of $K^0_S\pi^0_1$. (c) Invariant mass distribution of $\pi^0_S\pi^0_2$.

TABLE IV. Values of the parameters from the combined fit for the data of the decay $D^0 \to K_S^0\pi^0\pi^0$ with the $\bar{K}^*(1680)$ contributed and the energy-dependent parametrization of Eq. (22).

Parameters	C_1	α	D	D'	$\alpha_{\bar{K}^*(892)}$	D_1	D'_1	$\alpha'_{\bar{K}^*(892)}$
Fit	279.96	−5.80	463.88	−739.94	2.99	127.19	−841.02	−10.86

Parameters	$D_{\bar{K}^*(1680)}$	$D'_{\bar{K}^*(1680)}$	$\alpha_{\bar{K}^*(1680)}$	$D_{1,\bar{K}^*(1680)}$	$D'_{1,\bar{K}^*(1680)}$	$\alpha'_{\bar{K}^*(1680)}$	$\chi^2/\text{d.o.f.}$
Fit	4729.23	−3607.05	11.11	9596.12	−3324.87	−8.60	8.94

meson $\bar{K}^*(892)$ in the P wave, which also contribute to the one in the higher-energy region around 1.75GeV^2. The clear peak at 1.0GeV^2 is the signal of the scalar meson $f_0(980)$, which is dynamically generated from the S-wave pseudoscalar meson-pseudoscalar interactions. It should be mentioned that our results are consistent with the results obtained in Ref. [53].

From Table I, one can find that the fitted $\chi^2/\text{d.o.f} = 35.38$ (d.o.f. denoted as the degree of freedom) is big. To improve the fitting results, we try to take an energy-dependent parametrization for the P-wave amplitudes, written as

$$D \to D' \cdot s_{12} + D, \qquad D_1 \to D'_1 \cdot s_{13} + D_1, \quad (22)$$

with two more free parameters D' and D'_1 introduced. The obtained results are shown in Table II and Fig. 6, which are improved a lot with $\chi^2/\text{d.o.f.} = 10.81$, especially for the results of the two invariant mass distributions of $K_S^0\pi^0$, see Fig. 6. On the other hand, as found in the experiment [49], some other higher resonances are also contributed, such as the ones $\bar{K}_2^*(1430)$, $\bar{K}^*(1680)$, $f_2(1270)$, and so on. Since

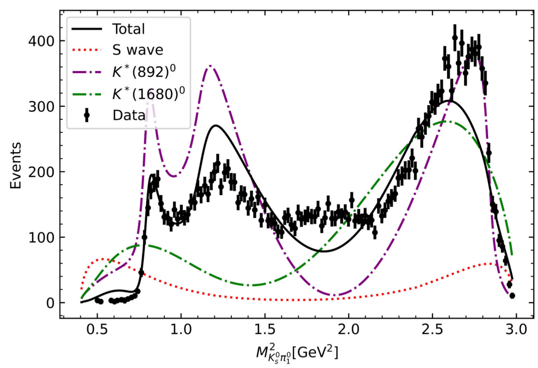

(a)

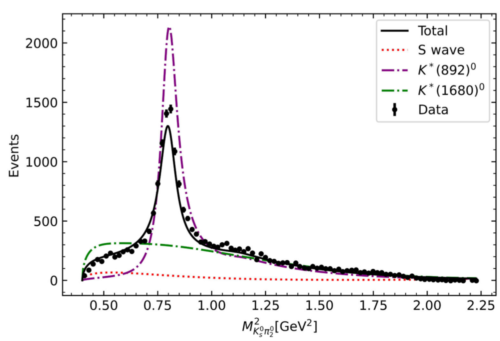

(b)

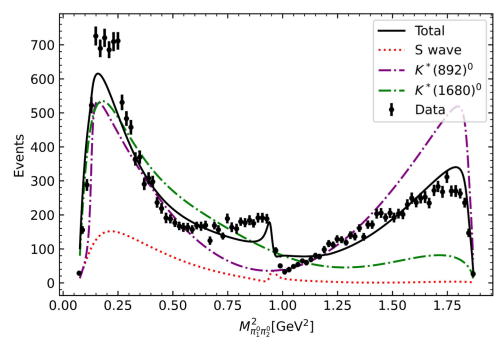

(c)

FIG. 8. Combined fit for the invariant mass distributions of the decay $D^0 \to K_S^0\pi^0\pi^0$ with the $\bar{K}^*(1680)$ contributed and the energy-dependent parametrization of Eq. (22). The solid (black) line is the total contributions of the S and P waves, the dashed (red) line represents the S-wave contributions, the dash-dotted (purple) line means the contributions of the $\bar{K}^*(892)$ in the P wave. The dotted (black) points are the experimental data measured by the BESIII Collaboration [49]. (a) Invariant mass distribution of $K_S^0\pi_1^0$. (b) Invariant mass distribution of $K_S^0\pi_2^0$. (c) Invariant mass distribution of $\pi_1^0\pi_2^0$.

TABLE V. Values of the parameters from the combined fit for the data of the $K_S^0\pi^0$, $K_S^0\eta$, and $\pi^0\eta$ spectra observed by the BESIII Collaboration [48].

Parameters	C_1	α	D	$\alpha_{\bar{K}^*(892)}$	$\chi^2/\mathrm{d.o.f.}$
Fit	3342.04	−3.38	138.31	2.34	11.59

the $\bar{K}^*(1680)$ resonance has a larger fit fraction, as shown in Table 4 of Ref. [49], we take its contribution into account, and thus, we add four more parameters due to two $\bar{K}^*(1680)$ being added. The fitted results of the parameters and invariant mass distributions are given in Table III and Fig. 7, where the $\chi^2/\mathrm{d.o.f.} = 12.99$ is also much improved and the line shapes in the low-energy parts of two $K_S^0\pi^0$ invariant mass distributions have been fitted well, see Fig. 7. Note that, to reduce theoretical uncertainties with less parameters, we do not consider the other higher resonances, which have small fit fractions as found in experiment [49]. Furthermore, we also consider the energy-dependent parametrization for four P-wave amplitudes, where four more parameters are explored. The results are presented in Table IV and Fig. 8, where the $\chi^2/\mathrm{d.o.f.} = 8.94$ is improved significantly. As clearly shown in Fig. 8, the low-energy parts of these three invariant mass distributions and the high-energy parts of the $K_S^0\pi_1^0$ invariant mass distributions describe the data much better with more clear signal of the $\bar{K}^*(1680)$ contribution, which in fact has small contribution, as found in experiment (see Table 4 and Fig. 4 of [49]). Thus, to match the experimental findings, maybe it is enough to fit data better to consider one of two cases, with higher resonance contribution or an energy-dependent parametrization for the P-wave amplitudes.

Similarly, for the $D^0 \to K_S^0\pi^0\eta$ process, in order to describe the $K_S^0\pi^0$, $K_S^0\eta$, and $\pi^0\eta$ invariant mass distributions simultaneously, we also make a combined fit to the experimental data of the BESIII Collaboration [48]. The fitted parameters are presented in Table V, and the invariant mass spectra are shown in Fig. 9, where we have taken into account the different bin sizes of the spectra, see the results of Ref. [48]. One can see that our fitting results are almost

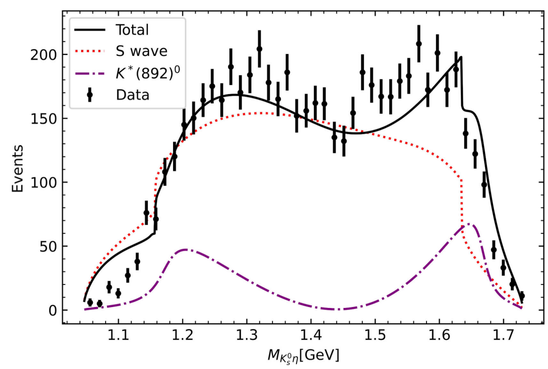

(a)

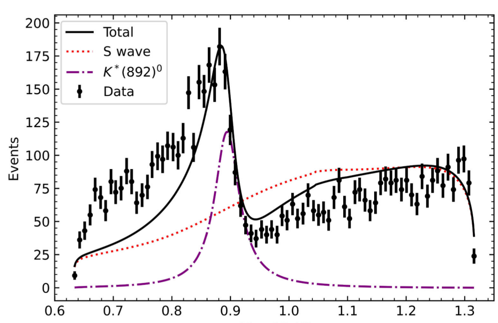

(b)

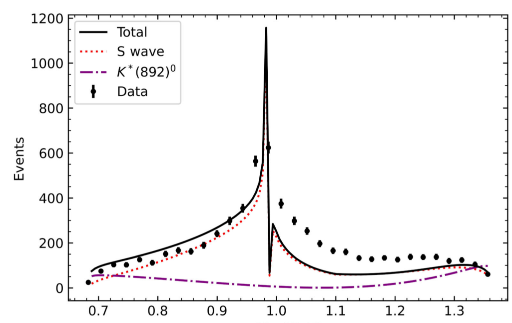

(c)

FIG. 9. Combined fit for the invariant mass distributions of the decay $D^0 \to K_S^0\pi^0\eta$. The solid (black) line is the total contributions of the S and P waves, the dashed (red) line represents the S-wave contributions, the dash-dotted (purple) line means the contributions of the $\bar{K}^*(892)$ in the P wave. The dotted (black) points are the experimental data measured by the BESIII Collaboration [48]. (a) Invariant mass distribution of $K_S^0\eta$. (b) Invariant mass distribution of $K_S^0\pi^0$. (c) Invariant mass distribution of $\pi^0\eta$.

TABLE VI. Values of the parameters from the combined fit for the data of the $K_S^0\pi^0$, $K_S^0\eta$, and $\pi^0\eta$ with the $\bar{K}^*(1410)$ contributed.

Parameters	C_1	α	D	$\alpha_{\bar{K}^*(892)}$	$D_{\bar{K}^*(1410)}$	$\alpha_{\bar{K}^*(1410)}$	$\chi^2/\mathrm{d.o.f.}$
Fit	3250.75	−4.52	124.54	2.53	−765.52	1.26	10.34

in agreement with experiments within the uncertainties. For the $K_S^0\eta$ mass distribution as shown in Fig. 9(a), there are double hump structures, which are the contributions of the interference effect between the S-wave amplitude and the P-wave one with the intermediate resonance $\bar{K}^*(892)$ and where the S-wave contribution is dominant. In Fig. 9(b), the structure around 0.9 GeV in the $K_S^0\pi^0$ spectrum is the contribution of the $\bar{K}^*(892)$, and the bump in the higher region benefits from the S wave. For the $\pi^0\eta$ invariant mass distribution as depicted in Fig. 9(c), the clear enhancement around 1.0 GeV is the signal of the $a_0(980)$, which is dynamically generated from the S-wave final state interactions regarded as a $K\bar{K}$ molecular state, and the contribution from the P wave is tiny.

Our fitted $\chi^2/\mathrm{d.o.f.} = 11.59$ is a bit large, since we do not consider the contributions from the other higher resonances, as considered in the experiment [48]. According to Table I of Ref. [48], the $\bar{K}^*(1410)$ had a larger fit fraction contribution compared to the others. Thus, with its contribution we remake the fit again with two more free parameters and obtain the results as given in Table VI and Fig. 10, where the fitted results are improved a bit with $\chi^2/\mathrm{d.o.f.} = 10.34$. As done above, here the other higher resonances are also ignored due to their small contributions [48]. Moreover, as done in the decay $D^0 \to K_S^0\pi^0\pi^0$ above, an energy-dependent parametrization is also taken into account to the both P-wave amplitudes by adding two more parameters, where the results are shown in Table VII and Fig. 11. From Table VII and Fig. 11, indeed, once again, we find that the fitted invariant mass distributions, especially the lower-energy parts of the $K_S^0\pi^0$, are significant improvements with $\chi^2/\mathrm{d.o.f.} = 6.73$ and more parameters. In Fig. 11, one can also see that the two P-wave resonances have obvious contributions, whereas the higher one had a small contribution as found in the

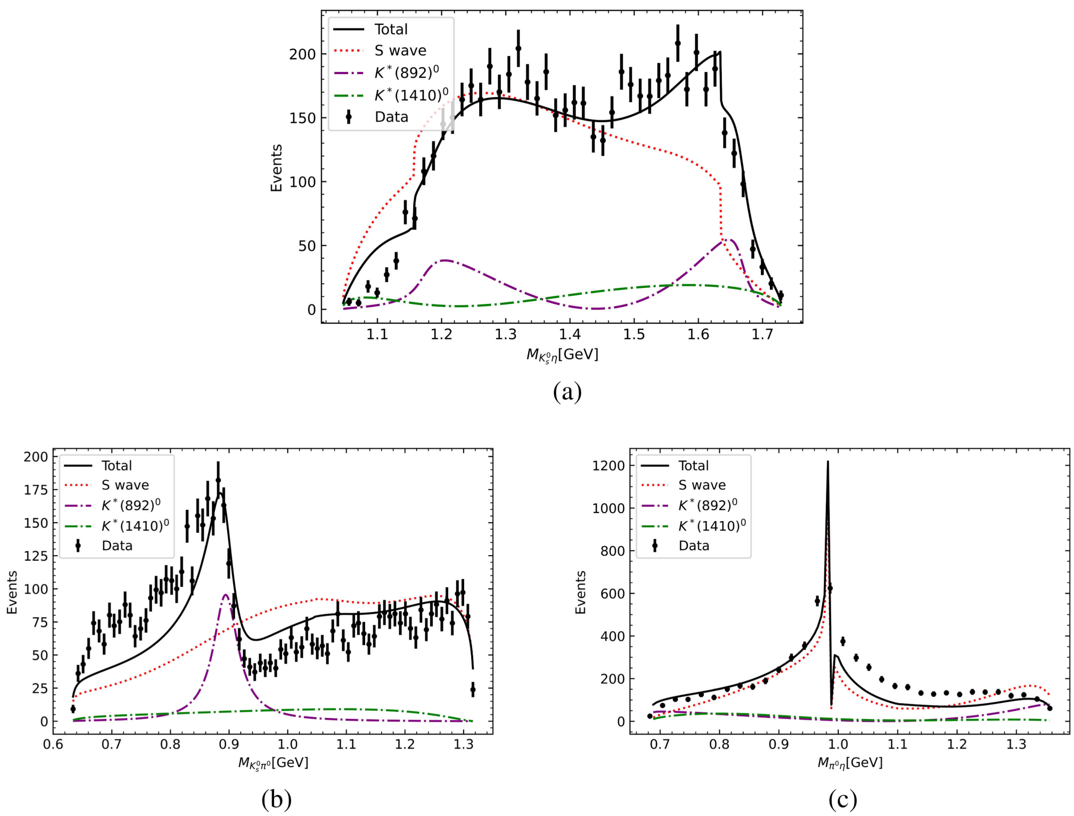

FIG. 10. Combined fit for the invariant mass distributions of the decay $D^0 \to K_S^0\pi^0\eta$ with the $\bar{K}^*(1410)$ contributed. The solid (black) line is the total contributions of the S and P waves, the dashed (red) line represents the S-wave contributions, the dash-dotted (purple) line means the contributions of the $\bar{K}^*(892)$ in the P wave. The dotted (black) points are the experimental data measured by the BESIII Collaboration [48]. (a) Invariant mass distribution of $K_S^0\eta$. (b) Invariant mass distribution of $K_S^0\pi^0$. (c) Invariant mass distribution of $\pi^0\eta$.

TABLE VII. Values of the parameters from the combined fit for the data of the $K_S^0\pi^0$, $K_S^0\eta$, and $\pi^0\eta$ with the $\bar{K}^*(1410)$ contributed and the energy-dependent parametrization.

Parameters	C_1	α	D	D'	$\alpha_{\bar{K}^*(892)}$	$D_{\bar{K}^*(1410)}$	$D'_{\mathrm{bar}K^*(1410)}$	$\alpha_{\bar{K}^*(1410)}$	χ^2/d.o.f.
Fit	4180.46	−0.96	1965.26	−2315.30	2.98	−5427.37	3065.76	2.40	6.73

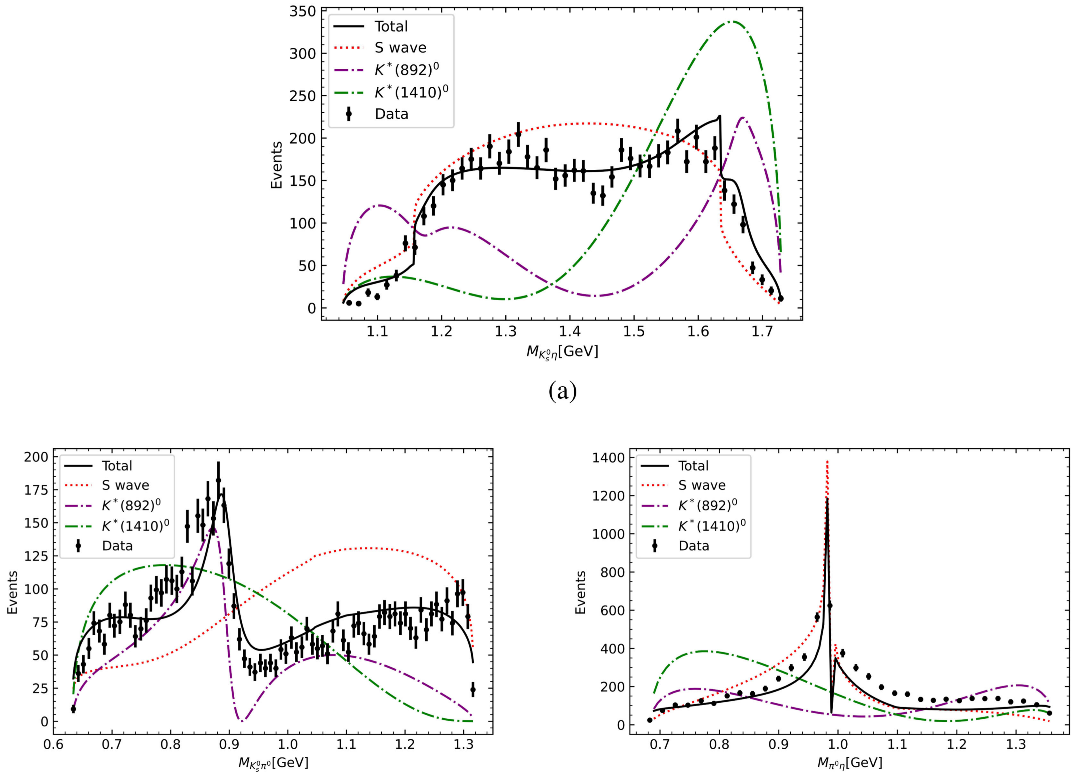

(a)

(b) (c)

FIG. 11. Combined fit for the invariant mass distributions of the decay $D^0 \to K_S^0\pi^0\eta$ with the $\bar{K}^*(1410)$ contributed and the energy-dependent parametrization. The solid (black) line is the total contributions of the S and P waves, the dashed (red) line represents the S-wave contributions, the dash-dotted (purple) line means the contributions of the $\bar{K}^*(892)$ in the P wave. The dotted (black) points are the experimental data measured by the BESIII Collaboration [48]. (a) Invariant mass distribution of $K_S^0\eta$. (b) Invariant mass distribution of $K_S^0\pi^0$. (c) Invariant mass distribution of $\pi^0\eta$.

experiment [48]. As the case of the $D^0 \to K_S^0\pi^0\pi^0$ above, these results also indicate that two cases, with higher resonance contribution and an energy-dependent parametrization for the P-wave amplitudes, are taken into account one of them enough to fit the data better.

IV. SUMMARY

Motivated by the BESIII Collaboration measurements for the decays $D^0 \to K_S^0\pi^0\eta$ and $D^0 \to K_S^0\pi^0\pi^0$, we investigate these two processes with the same weak decay diagram of internal-W emission mechanism in the quark level. For the final state interaction in the hadron level, we consider the S-wave pseudoscalar meson-pseudoscalar meson interaction within the chiral unitary approach, where the scalar resonances $f_0(500)$, $f_0(980)$, and $a_0(980)$ are dynamically generated. Moreover, the contributions from the P-wave intermediate vector meson $\bar{K}^*(892)$ and some other higher resonances are also taken into account. By considering the interference of the S- and P-waves amplitudes, we make a combined fit for corresponding invariant mass spectra, where the free parameters can be obtained and good descriptions of the experimental data can be achieved. For the decay $D^0 \to K_S^0\pi^0\eta$, the peak around 1.0 GeV in the $\pi^0\eta$ mass distribution is the signal of the $a_0(980)$, while the contribution of intermediate resonance $\bar{K}^*(982)$ in this distribution is very small and just as a background. For the process $D^0 \to K_S^0\pi^0\pi^0$, the obvious structure around 1.0GeV^2 in the $\pi_1^0\pi_2^0$ mass spectrum is associated with the $f_0(980)$, which is dynamically generated from the S-wave coupled channel interactions, and the bump at low region benefits from the contributions of $f_0(500)$ and $\bar{K}^*(892)$. Furthermore, to improve the fits, we also consider the contributions from some higher resonances as found in the experiments and an energy-dependent parametrization to the parameters of the P-wave amplitudes. The obtained results indicate that the fitted results are better in each case. When two cases are taken into account simultaneously, the results are improved significantly with more parameters and clear higher-energy resonances contributed significantly, which do not match the results as found in the experiment and indicate that it is enough to consider one of them.

ACKNOWLEDGMENTS

We are thankful for useful discussions with Professor Bai-Cian Ke. This work is supported by the Natural Science Foundation of Guangxi province under Grant No. 2023JJA110076, the Natural Science Foundation of Hunan province under Grant No. 2023JJ30647, and the National Natural Science Foundation of China under Grants No. 12365019 and No. 12575081.

DATA AVAILABILITY

There are no publicly available research data or software supporting this manuscript. Requests for further information or data should be sent to the authors.

[1] H. Y. Cheng, Int. J. Mod. Phys. Conf. Ser. **02**, 61 (2011).
[2] H. Y. Cheng and C. W. Chiang, Phys. Rev. D **81**, 074021 (2010).
[3] S. Navas *et al.* (Particle Data Group), Phys. Rev. D **110**, 030001 (2024).
[4] H. X. Chen, W. Chen, X. Liu, and S. L. Zhu, Phys. Rep. **639**, 1 (2016).
[5] A. Hosaka, T. Iijima, K. Miyabayashi, Y. Sakai, and S. Yasui, Prog. Theor. Exp. Phys. **2016**, 062C01 (2016).
[6] F. K. Guo, C. Hanhart, U.-G. Meißner, Q. Wang, Q. Zhao, and B. S. Zou, Rev. Mod. Phys. **90**, 015004 (2018).
[7] A. Esposito, A. Pilloni, and A. D. Polosa, Phys. Rep. **668**, 1 (2016).
[8] S. L. Olsen, T. Skwarnicki, and D. Zieminska, Rev. Mod. Phys. **90**, 015003 (2018).
[9] C. Z. Yuan, Int. J. Mod. Phys. A **33**, 1830018 (2018).
[10] N. Brambilla, S. Eidelman, C. Hanhart, A. Nefediev, C. P. Shen, C. E. Thomas, A. Vairo, and C. Z. Yuan, Phys. Rep. **873**, 1 (2020).
[11] W. F. Wang, Phys. Rev. D **104**, 116019 (2021).
[12] Y. Li, S. W. Liu, E. Wang, D. M. Li, L. S. Geng, and J. J. Xie, Phys. Rev. D **110**, 074010 (2024).
[13] F. E. Close and N. A. Tornqvist, J. Phys. G **28**, R249 (2002).
[14] V. R. Debastiani, W. H. Liang, J. J. Xie, and E. Oset, Phys. Lett. B **766**, 59 (2017).
[15] W. H. Liang, J. J. Xie, and E. Oset, Eur. Phys. J. C **76**, 700 (2016).
[16] J. Y. Wang, M. Y. Duan, G. Y. Wang, D. M. Li, L. J. Liu, and E. Wang, Phys. Lett. B **821**, 136617 (2021).
[17] X. C. Feng, L. L. Wei, M. Y. Duan, E. Wang, and D. M. Li, Phys. Lett. B **846**, 138185 (2023).
[18] Z. Wang, Y. Y. Wang, E. Wang, D. M. Li, and J. J. Xie, Eur. Phys. J. C **80**, 842 (2020).
[19] S. Godfrey and N. Isgur, Phys. Rev. D **32**, 189 (1985).
[20] D. Morgan and M. R. Pennington, Phys. Rev. D **48**, 1185 (1993).
[21] N. A. Tornqvist and M. Roos, Phys. Rev. Lett. **76**, 1575 (1996).
[22] H. J. Lee, New Phys. Sae Mulli **72**, 887 (2022).
[23] R. L. Jaffe, Phys. Rev. D **15**, 267 (1977).
[24] B. S. Zou and D. V. Bugg, Phys. Rev. D **50**, 591 (1994).
[25] G. Janssen, B. C. Pearce, K. Holinde, and J. Speth, Phys. Rev. D **52**, 2690 (1995).
[26] J. A. Oller and E. Oset, Nucl. Phys. **A620**, 438 (1997); **A652**, 407(E) (1999).
[27] M. P. Locher, V. E. Markushin, and H. Q. Zheng, Eur. Phys. J. C **4**, 317 (1998).
[28] V. Baru, J. Haidenbauer, C. Hanhart, Y. Kalashnikova, and A. E. Kudryavtsev, Phys. Lett. B **586**, 53 (2004).
[29] R. Albuquerque, S. Narison, and D. Rabetiarivony, Nucl. Phys. **A1039**, 122743 (2023).
[30] E. Oset and A. Ramos, Nucl. Phys. **A635**, 99 (1998).
[31] G. Toledo, N. Ikeno, and E. Oset, Eur. Phys. J. C **81**, 268 (2021).
[32] J. A. Oller and U. G. Meissner, Phys. Lett. B **500**, 263 (2001).
[33] F. K. Guo, R. G. Ping, P. N. Shen, H. C. Chiang, and B. S. Zou, Nucl. Phys. **A773**, 78 (2006).
[34] R. Aaij *et al.* (LHCb Collaboration), J. High Energy Phys. 04 (2019) 063.
[35] M. Ablikim *et al.* (BESIII Collaboration), Phys. Rev. Lett. **124**, 241803 (2020).
[36] P. del Amo Sanchez *et al.* (*BABAR* Collaboration), Phys. Rev. Lett. **105**, 081803 (2010).
[37] L. K. Li *et al.* (Belle Collaboration), J. High Energy Phys. 09 (2021) 075.
[38] M. Ablikim *et al.* (BESIII Collaboration), Phys. Rev. D **101**, 052009 (2020).
[39] M. Artuso *et al.* (CLEO Collaboration), Phys. Rev. D **77**, 092003 (2008).
[40] M. Ablikim *et al.* (BESIII Collaboration), Phys. Rev. D **110**, L111102 (2024).

[41] Z. Y. Wang, H. A. Ahmed, and C. W. Xiao, Phys. Rev. D **105**, 016030 (2022).
[42] W. H. Liang, J. J. Xie, and E. Oset, Phys. Rev. D **92**, 034008 (2015).
[43] J. J. Xie and E. Oset, Phys. Rev. D **90**, 094006 (2014).
[44] X. Z. Ling, M. Z. Liu, J. X. Lu, L. S. Geng, and J. J. Xie, Phys. Rev. D **103**, 116016 (2021).
[45] Y. Ding, E. Wang, D. M. Li, L. S. Geng, and J. J. Xie, Phys. Rev. D **110**, 014032 (2024).
[46] Y. Ding, X. H. Zhang, M. Y. Dai, E. Wang, D. M. Li, L. S. Geng, and J. J. Xie, Phys. Rev. D **108**, 114004 (2023).
[47] L. R. Dai, Q. X. Yu, and E. Oset, Phys. Rev. D **99**, 016021 (2019).
[48] M. Ablikim *et al.* (BESIII Collaboration), arXiv:2512.23389.
[49] M. Ablikim *et al.* (BESIII Collaboration), arXiv:2510.25111.
[50] P. Rubin *et al.* (CLEO Collaboration), Phys. Rev. Lett. **93**, 111801 (2004).
[51] N. Lowrey *et al.* (CLEO Collaboration), Phys. Rev. D **84**, 092005 (2011).
[52] J. J. Xie, L. R. Dai, and E. Oset, Phys. Lett. B **742**, 363 (2015).
[53] X. H. Zhang, H. Zhang, B. C. Ke, L. J. Liu, D. M. Li, and E. Wang, Phys. Rev. D **110**, 114050 (2024).
[54] N. Ikeno, J. M. Dias, W. H. Liang, and E. Oset, Eur. Phys. J. C **84**, 469 (2024).
[55] M. Ablikim *et al.* (BESIII Collaboration), Phys. Rev. Lett. **132**, 131903 (2024).
[56] Y. Q. Chen *et al.* (Belle Collaboration), Phys. Rev. D **102**, 012002 (2020).
[57] A. Martinez Torres, L. S. Geng, L. R. Dai, B. Sun, Xi, E. Oset, and B. S. Zou, Phys. Lett. B **680**, 310 (2009).
[58] A. Bramon, A. Grau, and G. Pancheri, Phys. Lett. B **283**, 416 (1992).
[59] L. Roca, J. E. Palomar, and E. Oset, Phys. Rev. D **70**, 094006 (2004).
[60] D. Gamermann, E. Oset, and B. S. Zou, Eur. Phys. J. A **41**, 85 (2009).
[61] R. Molina, J. J. Xie, W. H. Liang, L. S. Geng, and E. Oset, Phys. Lett. B **803**, 135279 (2020).
[62] W. H. Liang and E. Oset, Phys. Lett. B **737**, 70 (2014).
[63] Z. Y. Wang, J. Y. Yi, Z. F. Sun, and C. W. Xiao, Phys. Rev. D **105**, 016025 (2022).
[64] H. A. Ahmed, Z. Y. Wang, Z. F. Sun, and C. W. Xiao, Eur. Phys. J. C **81**, 695 (2021).
[65] W. Liang, J. Y. Yi, C. W. Xiao, and S. Q. Zhou, Phys. Rev. D **108**, 116001 (2023).
[66] C. W. Xiao, U.-G. Meißner, and J. A. Oller, Eur. Phys. J. A **56**, 23 (2020).
[67] W. H. Liang, J. J. Xie, and E. Oset, Eur. Phys. J. C **75**, 609 (2015).
[68] L. R. Dai, E. Oset, and L. S. Geng, Eur. Phys. J. C **82**, 225 (2022).
[69] J. A. Oller and E. Oset, Phys. Rev. D **60**, 074023 (1999).
[70] D. Gamermann, E. Oset, D. Strottman, and M. J. Vicente Vacas, Phys. Rev. D **76**, 074016 (2007).
[71] J. X. Lin, J. T. Li, S. J. Jiang, W. H. Liang, and E. Oset, Eur. Phys. J. C **81**, 1017 (2021).
[72] J. A. Oller, E. Oset, and A. Ramos, Prog. Part. Nucl. Phys. **45**, 157 (2000).
[73] L. Roca and E. Oset, Phys. Rev. D **103**, 034020 (2021).